JOURNAL OF AIRCRAFT
Vol. 45, No. 2, March–April 2008

Multidisciplinary Integrated Preliminary Design Applied to Unconventional Aircraft Configurations

Christian Werner-Westphal,* Wolfgang Heinze,† and Peter Horst‡
Technische Universitaet Braunschweig, 38108 Brunswick, Germany

DOI: 10.2514/1.32138

A preliminary aircraft design tool is presented as a means of performing multidisciplinary, integrated preliminary design of unconventional aircraft configurations. Higher fidelity numerical methods for some of the involved disciplines are discussed as key elements of this process. A noise propagation module is described as a first step toward introducing aircraft noise analysis into the preliminary design process. Application of the tool to a specific unconventional aircraft concept is shown. The results of this study provide an understanding of why multidisciplinary design analysis and optimization, as well as higher fidelity methods, are required for the design of unconventional aircraft configurations.

Nomenclature

$C_{A/C}$	=	life-cycle costs generated by the aircraft (purchase, depreciation, insurance, spares procurement)
C_{CREW}	=	life-cycle costs of cockpit and cabin crew
C_{FEES}	=	life-cycle costs of fees and charges
C_{FUEL}	=	life-cycle costs of fuel
C_{MRO}	=	life-cycle costs of maintenance, repair, and overhaul
c_{DISP}	=	specific cost factor for dispatch
c_{LDG}	=	specific cost factor for landing
c_p	=	aerodynamic pressure coefficient
D	=	drag force
$\boldsymbol{F}^{(e)}$	=	vector of forces at nodes of finite element
$\mathbf{J}$	=	Jacobian matrix
L	=	lift force
$\mathbf{N}$	=	matrix of form finite element form functions
N_F	=	number of total flights during aircraft life cycle
N_{PAX}	=	number of passenger seats in the aircraft
$\boldsymbol{n}^{(e)}$	=	normal vector of finite element
q	=	aerodynamic head
R	=	aircraft range
r, s	=	normalized finite element coordinates
t_{GND}	=	turnaround time
$t_{\max}$	=	maximum available aircraft operation time per year
u	=	annual utilization
V_C	=	cruise speed
x_{CG}	=	X component of aircraft center of gravity position
x_N	=	X component of aircraft aerodynamic center
x_{NW}	=	X component of wing aerodynamic center
y^*	=	number of years in service

Presented as Paper 0655 at the 45th AIAA Aerospace Sciences Meeting & Exhibit, Reno, NV, 8–11 January 2007; received 14 May 2007; revision received 13 August 2007; accepted for publication 25 October 2007.

*Research Assistant, Institute of Aircraft Design and Lightweight Structures, Hermann-Blenk-Straße 35; c.werner-westphal@tu-bs.de. AIAA member.

†Senior Researcher, Institute of Aircraft Design and Lightweight Structures, Hermann-Blenk-Straße 35; w.heinze@tu-bs.de.

‡Professor, Head of Institute, Institute of Aircraft Design and Lightweight Structures, Hermann-Blenk-Straße 35; p.horst@tu-bs.de.

I. Introduction

IN FUTURE transport aircraft development, new requirements (e.g., environmental considerations such as community noise and emission limits) are expected to play an ever increasing role, up to the extent where they will become driving parameters for a given aircraft design. This has mainly two consequences: first, new criteria emerge by which an aircraft design has to be judged; second, an aircraft design may have to undergo changes in configuration to fulfill the requirements. Because the classic economic and technical design targets and constraints are still in place, the only way to comply with the new criteria without overly penalizing the aircraft is to account for them as early in the design process as possible, which means considering them during the preliminary design phase.

Considering additional requirements in the preliminary design process has far-reaching effects, mostly due to the two consequences mentioned in the preceding paragraph: if new criteria are to be used for judging an aircraft design, methods allowing quantification and analysis of these criteria have to be implemented in the process. And, if new constraints lead to unconventional aircraft configurations, accurate results are unlikely to be obtained with existing statistical approaches and handbook methods, on which preliminary design and optimization processes traditionally rely. Instead, higher fidelity methods are needed to simulate actual, physical parameter dependencies.

In the field of aerospace, multidisciplinary design analysis (MDA) and optimization (MDO) has been applied for some time [1]. In general, MDA/MDO is beneficial when the system being designed is complex and has strong interactions between disciplines. It allows the simultaneous manipulation of variables in several disciplines and thus enables the design of systems that are highly optimized with regard to all main disciplines [1,2].

Regarding aircraft design, the increasing amount of constraints adds more complexity to an already complex design task. For conventional aircraft, much of this complexity can be spared by using suitable empirical models. However, for unconventional aircraft configurations, empirical models are usually not available. The combination of higher fidelity models (more physics) and multidisciplinary design tools (more complexity) becomes necessary.

At the Institute of Aircraft Design and Lightweight Structures (IFL), such a multidisciplinary integrated preliminary aircraft design and optimization tool has been under development for over 20 years [3,4]. Being of highly modular nature, this tool can easily be expanded, and the methods used for a certain task can easily be exchanged. This has allowed for the introduction of a noise propagation analysis module, allowing the consideration of aircraft noise as a new criterion. It has also allowed for the implementation of higher fidelity methods for aerodynamic and structural analysis [5,6], making the tool capable of accurately analyzing unconventional

aircraft configurations. The tool is presented in this paper, paying special attention to the implemented higher fidelity methods and the potential they have for further improving the design process. The capabilities of the tool are illustrated by discussing its application to a specific unconventional aircraft concept.

II. Preliminary Aircraft Design Process

An overview of the preliminary aircraft design and optimization tool (PrADO) is given in Fig. 1. The core of the tool is a set of independent computer codes, the design modules, each of which fulfills a specific task in the design process (e.g., module 2: fuselage geometry conversion, module 17: calculation of flight performance data for flight with maximum payload, etc.). These modules access configuration data through a common library called Data Management System (DMS), which includes a set of routines for reading and writing data from and to the database files, respectively. Different design modules communicate with each other only through the DMS. The database files, thematically sorted ASCII files containing all information relevant to the current design problem, are initially constructed from user input, which is provided in the form of an ASCII file and has to include the transport mission, a basic parametric description of the configuration layout, and all relevant constraints and design targets.

PrADO has three modes of operation. The first, design analysis, iteratively executes the complete sequence of design modules until convergence of all dependent design parameters is reached. The second mode, parameter variation, accepts user input of independent parameters to be varied within user-chosen limits. A complete design analysis (see preceding paragraph) is then performed for each set of independent parameters. This way, the entire design space can be illustrated and the user is given an overview of possible solutions. The third mode, optimization, finally, requires the definition of independent design variables, a target function [e.g., direct operating cost (DOC)], and design boundaries. An optimization algorithm is then used to search for design variable combinations that optimize (i.e., minimize or maximize) the target function. Underway, complete design analyses are performed for different variable configurations to assess the value of the target function.

Results of PrADO are output as a set of ASCII files containing all relevant data, but also as input files for visualization using the commercial program TecPlot [7]. The user may interact with the process and with the data through a convenient graphical user interface (GUI).

As a result of its structure, PrADO features a set of important qualities. Its modular structure makes it extremely flexible, as the process itself can be applied to basically any design problem. Because all modules are considered on the same level of an iterative process, the tool becomes truly multidisciplinary as soon as design modules pertaining to different disciplines are used. The exchange of data between all modules makes it an integrated process, in which every module may influence any other. Furthermore, the parametric description of the design problem allows for a great range of configuration variability without having to abandon the automated process.

In the past, PrADO has been validated for conventional aircraft configurations and used for different unconventional configurations (e.g., blended wing body, hydrogen fueled airplane, airship), as shown in [2,3]. An example of the geometry model for a typical passenger transport aircraft, as represented in PrADO, is shown in Fig. 2. As can be seen, the geometry model includes structural elements (e.g., skins, frames, spars, ribs), control surfaces, fuel tanks, as well as the complete cabin layout with seats, galleys, restrooms, and separation walls. The landing gear can be shown both in extended and retracted positions. Geometry models of humans, cargo containers, and ground vehicles are also available, making it possible to judge the ergonomic qualities of the cabin and the aircraft/airport integration.

One advantage of PrADO's modularity is the possibility to implement different methods for one task. Over time, different methods have been implemented for several key disciplines, among which the user may choose the ones to be used for a given design problem. In module 12, responsible for calculating the aerodynamic characteristics of the aircraft, for example, the choices include a simple analytical aerodynamic model, a multiple lifting line method [8], and a panel method. In module 21, responsible for calculating the operational empty weight (OEW), the user is able to choose for each part of the aircraft from a broad repertoire of methods, ranging from

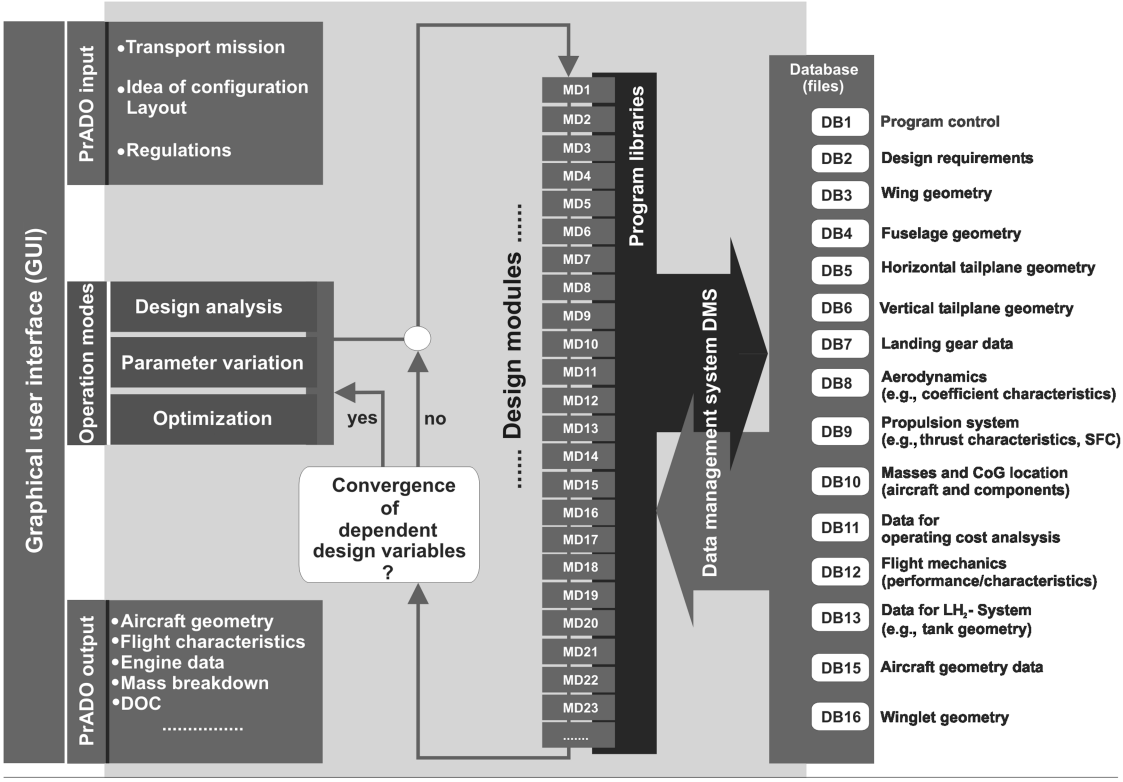

Fig. 1 PrADO process overview.

Fig. 2 Typical PrADO aircraft geometry model.

simple statistical interpolation methods to handbook methods found in the literature (e.g., the fuselage weight prediction method by Burt–Phillips [9]) up to finite element (FE) analysis.

Choosing FE analysis, which can presently be done for fuselage, wing, horizontal tail plane, and vertical tail plane, causes module 21 to run the "structural, aerodynamic, and aeroelastic analysis module" (SAM) [5,6]. Being independent in principle, SAM was designed to run as part of PrADO. It performs structural sizing by means of finite-element-based fully stressed design. The aerodynamic loads necessary for this are calculated using an aerodynamic panel code. Figure 3 gives an overview of the program structure. SAM consists of a control program [the structural sizing module (SSM)], a multimodel generator (MMG), an FE-preprocessor (FEMPRE), an in-house FE code (EFEM), and an FE-postprocessor (FEMPOST). The aerodynamic panel code used is the higher order subsonic/supersonic singularity method (HiSSS) [10], provided by the European Aeronautic Defense and Space Company, military branch (EADS-M), Munich.

The load cases used for structural sizing include flight points at the edges of the flight envelope, as well as cases of landing impact, and are provided by SSM. For each landing impact load case (a combination of payload and fuel distribution), zero aerodynamic lift is assumed. The maximum landing gear reaction force is calculated assuming a symmetrical 10 ft/s landing impact on all main landing gears, and considering the dynamic behavior of the landing gear spring and dampener system. The resulting maximum load factor is applied to all mass inertia forces.

For each flight load case (a combination of speed, altitude, and payload/fuel distribution), both the maneuver and the gust flight envelopes are evaluated, and the maximum load factor is selected. With this load factor, the required values for lift and momentum coefficient (C_L and C_M in Fig. 3) can be attained. Aerodynamic loads for each flight load case are then computed iteratively for trimmed flight, and are subsequently transferred to the FE model by FEMPRE. During load transfer, the aerodynamic pressure coefficients c_p for all panels have to be converted into explicit forces at the nodes of the structural model. The difficulty of this approach is that both meshes represent different discretizations of the aircraft geometry and have different node positions. Additionally, the structural model does not

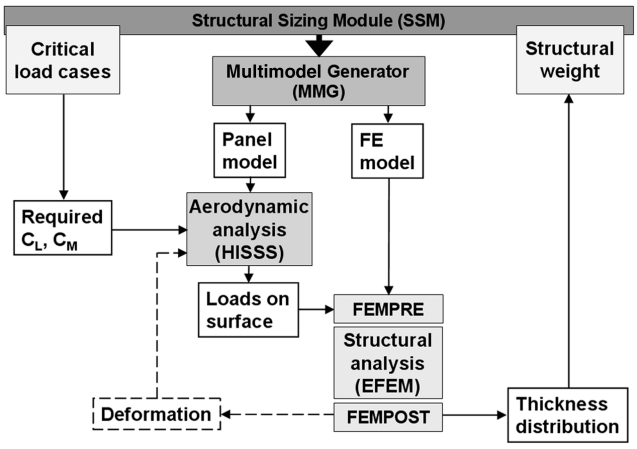

Fig. 3 SAM program structure.

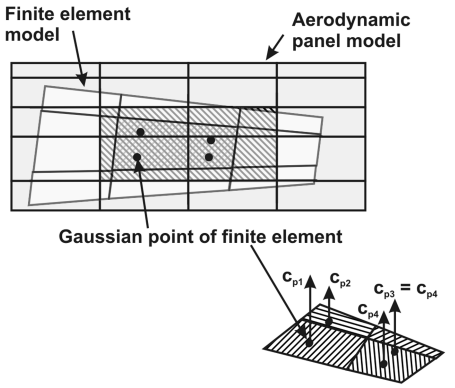

Fig. 4 Projection of structural mesh on aerodynamic mesh.

cover the whole surface of the aircraft (e.g., in the wing, only the wing box is modeled explicitly, with leading- and trailing-edge devices represented as nonstructural mass elements). However, all structural elements lying on the surface are quadrilateral isoparametric shell elements. Therefore, each Gaussian point of each element can be projected onto one aerodynamic panel (see Fig. 4). The pressure coefficient on this panel is taken as the pressure coefficient for the corresponding Gaussian point. For parts of the surface not covered by the structural model (e.g., the leading and trailing edges of lifting surfaces), virtual elements are created. The forces at the nodes can then be calculated with Eq. (1).

$$\boldsymbol{F}^{(e)} = \boldsymbol{n}^{(e)} q \iint c_p(r,s) \det \mathbf{JN}\, \mathrm{d}r\, \mathrm{d}s \tag{1}$$

$\boldsymbol{F}^{(e)}$ represents the vector of forces at the element nodes, $\boldsymbol{n}^{(e)}$ is the normal vector of the element, q is the total aerodynamic head, $\mathbf{J}$ is the Jacobian matrix, and $\mathbf{N}$ is the matrix of form functions, as shown in Eq. (2).

$$\begin{aligned} N_1 &= \frac{1}{4}(1+r)(1+s) \qquad N_2 = \frac{1}{4}(1-r)(1+s) \\ N_3 &= \frac{1}{4}(1-r)(1-s) \qquad N_4 = \frac{1}{4}(1+r)(1-s) \end{aligned} \tag{2}$$

The parameters r and s represent the normalized element coordinate system, and have values between zero and one. By applying Gaussian quadrature, Eq. (1) can be solved using only the values for c_p and $\mathbf{N}$ for the coordinates of the Gaussian points. This is done for all elements, including the virtual elements. Forces from nodes on virtual elements are then transferred to the structural mesh assuming rigid coupling. Finally, because the numeric integration of aerodynamic loads is not exact, all forces are scaled with a global factor to provide the required amount of total lift.

Other loads considered in flight load cases include inertial forces of engines, landing gear, payload and fuel, and cabin pressure loads.

The structural weight of the chosen components is calculated by integrating the distributed wall thickness, which results from the iterative FE sizing process. All load cases are considered simultaneously and, for each element, the maximum wall thickness required by any load case is chosen.

The key to the flexibility of the high-fidelity methods is the MMG, which automatically generates both a panel model of the aircraft contour (for use in HiSSS) and a finite element representation of the aircraft structure (for use in EFEM). To reduce the computational effort, half-models are used, assuming aircraft and load case symmetry. MMG is documented in more detail in [5,6]. The common basis for both models is the parametric geometry description available in the PrADO database files. From this description, a surface spline representation is generated for each aircraft component [fuselage(s), wing(s), vertical and horizontal tail planes, and winglets if present]. The following steps are performed separately for each component. From the surface spline representation, nodes for both meshes are extracted. Additional nodes for the structural mesh (e.g., interior nodes for the fuselage

bulkheads, which do not lie on the surface) are then generated. For the aerodynamic mesh, node connectivity information and subnet structure are generated. For the structural mesh, element properties are generated from stored data sets. In the next step, the component meshes are assembled to a global configuration. For this, the component meshes have to be modified, and double nodes have to be deleted. For the structural model, connecting elements have to be defined. Different subroutines exist with basic solutions for mesh topology depending on the kind of component connection (e.g., low-wing, high-wing, t-tail, etc.). These are applied to the actual parameters and dimensions of the configuration. In the structural model, other aircraft components are considered as nonstructural masses (engines, landing gear) or as simplified beam structures (pylon). After assembly, the wake surfaces for the aerodynamic panel model are generated before the resulting models are output in ASCII format.

An interesting feature of the described process is that the influence of static aeroelasticity can easily be considered, simply by providing a feedback of FE deformation results into the aerodynamic panel model, thereby closing an additional iteration loop. The conversion from node displacements in the structural model into node displacements in the aerodynamic model is accomplished by interpolation using a spline function [3]. Of course, this is done at the expense of a significantly increased computational effort.

As a first step toward assessing environmentally friendly technologies, a noise propagation module has been implemented into the process [11,12]. The basic idea is that a point source representing the overall aircraft is moved along a flight path simulating departure or approach, while the emitted noise is propagated numerically and integrated on the ground over the surrounding area, leading to characteristic noise contour plots. Effects considered in noise propagation include source directivity, spheric dispersion, atmospheric attenuation, ground attenuation, Doppler effect (noise level shift only), and ground reflection. Additionally, noise levels for the classic certification measurement points (departure, sideline, and approach) are also computed. Different metrics are available for noise level output [dBA (A-weighted decibels), EPNdB (effective perceived noise decibels), see [13] for further information]. By varying flight-path parameters (e.g., departure climb angle) in accordance with aircraft capabilities (e.g., thrust-to-weight ratio), influences of design changes on the noise footprint can be made visible.

As reported in [13], noise contour plots have been used for a long time, although mainly to visualize community noise impact in airport-centered analyses. The author advocates the use of contour-based methodologies in the aircraft certification process, stating that this would provide a certification system more closely related to the actual operational noise impact of an aircraft than the current system of fixed measurement points. The difficulties of computing contours with accuracy and of validating them experimentally are seen as the main drawbacks [13]. For the purposes of an integrated multidisciplinary aircraft design tool, such as PrADO, visualizing the changes caused in the noise characteristics of a given design by modifications of design and/or operational parameters is more important than the exact prediction of absolute noise levels. For this purpose, noise contours provide much more information than noise levels at the certification points, even if this information is mostly qualitative.

Although the noise module is operational in its present form, it requires a noise source description of the aircraft to be provided by the user. The noise source is independent of aircraft parameters other than thrust setting and thus does not change during the design process. In the future, it is intended to complete the noise module by adding a parametric noise source model that considers airframe and engine noise, as well as installation and noise shielding effects. In the first development step, it is intended to use mostly empirical methods such as those included in NASA Langley Research Center's Aircraft Noise Prediction Program (ANOPP) [14] or those included in the Engineering Sciences Data Unit's (ESDU) Aircraft Noise Series.[§]

[§]http://www.esdu.com [retrieved 09 August 2007].

A complete PrADO design analysis of a given configuration with FE-based structural sizing takes around 6–8 h to compute on a 3 GHz Pentium 4 PC with 1 GB RAM and Microsoft Windows XP operating system, depending on the size of the aircraft. A typical aerodynamic model generated by MMG contains approximately 2500–4000 panels, and a typical finite element model contains approximately 3000–10,000 nodes, depending on aircraft size. The process of design analysis is fully automatic once the PrADO input file has been set up and the computation has been started. Computation time for design analysis increases to approximately 3–5 days if static aeroelasticity is to be considered, but can be reduced to as little as approximately 45 min. if low-fidelity methods are used for all disciplines.

III. Application Examples

Because of the aforementioned limitations, it is currently possible to perform noise analysis only for design cases in which a noise source description is available. Such a noise source description is not yet available for the unconventional aircraft concept discussed in Sec. III.B, and so noise analysis is not described in this context. Instead, Sec. III.A illustrates the functionality of the noise propagation module with results obtained for a conventional transport aircraft.

A. Sample Noise Propagation Module Results

Figure 5 [12] shows resulting noise footprints in dBA, obtained with the noise propagation module in PrADO. These results correspond to the takeoff of a twin engine 150-seat conventional passenger transport aircraft (dubbed P150) and were calculated on a 50×50 m mesh in time steps of 0.5 s. The similarity of the contours to the ones found in the literature (e.g., [13], p. 243) is apparent. As can be seen, changes in departure climb angle immediately affect the size of the 85dBA contour, with the noise-affected area decreasing as the aircraft climbs away from the ground more rapidly. Note that, in this case, both departures were performed with the same power settings, varying aircraft speed instead.

As far as the underlying physics are concerned, Fig. 5 shows a typical noise contour shape for takeoff of a single conventional aircraft. The footprint has a very characteristic form. As the aircraft stands on the runway before takeoff, noise is emitted mostly at an angle of 100–120 deg from the direction the aircraft is heading, causing the two visible lobes. As the aircraft accelerates after brake release, the contour slims because engine noise decreases with decreasing relative speed between the engine exhaust jet and the air around it. After liftoff, the effects of ground attenuation decrease progressively, causing the contour to widen again, up to a point where the increasing distance from the ground becomes the predominant factor, causing noise levels to decrease. If thrust cutback is used, the contour is slimmed instantly, but a zone of

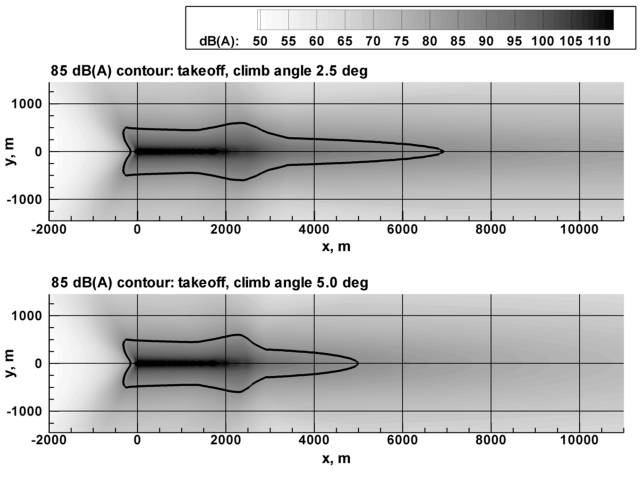

Fig. 5 Example noise contour plots for takeoff.

Table 1 Noise propagation module results validation

Noise levels in EPNdB		
Certification point	PrADO P150 noise level	Airbus A320-200 noise level
Takeoff	91.14	~84–88[a]
Sideline	99.20	~96–97[a]

[a]Depending on max. weight and engine selection

increased ground noise may arise when full power is restored for climb later on (not visible in this case).

Validation of the overall absolute noise level values predicted by the module is rather difficult. Table 1 shows noise levels obtained for the P150 at the takeoff certification points (in EPNdB), compared with published noise levels for the Airbus A320–200 [15], an aircraft similar to the P150 in configuration, size, and weight. As can be seen, the absolute noise levels agree well considering the actual complexity of the problem and the rather simple approach taken. Furthermore, the inaccuracies are deemed to be caused mainly by deficiencies of the available noise source description. Although the noise source could easily be calibrated to match A320 results, only the effects of operational changes (e.g., climb angle or use of thrust cutback) can currently be studied. Once a parametric source model is implemented as discussed in Sec. II, noise levels at the source will become a function not only of power setting, but also of aircraft configuration, flap and slat settings, landing gear position, and other factors. The flight simulation will then be able to create a direct link between the aircraft's climbing performance and the community noise associated with it.

B. Low-Noise Aircraft Concept Analysis

1. Configuration Overview and Baseline Results

As an illustrating example of PrADO's and SAM's capabilities, some of the results obtained for an unconventional aircraft concept are to be analyzed and discussed. The configuration for this study was developed at the Institute of Aerodynamics and Flow Technology (AS) of the German Aerospace Center (DLR) as a low-noise aircraft concept (and is therefore dubbed LNA here), and has been analyzed at IFL. The LNA is a 260 passenger, twin-engine subsonic transport aircraft with a design range of 6500 km at a cruise speed of Mach 0.8. Figure 6 shows the external geometry model for this aircraft concept. The overall configuration includes the following features, intended to minimize community noise impact (also listed in Fig. 6): 1) engines mounted above the wing to enable downward engine noise shielding by the wing; 2) double fins instead of a vertical tail plane, mounted outboard of the engines to provide noise shielding; 3) forward swept outer wings for improved shielding of fan noise; 4) increased wing reference area for increased noise shielding surface (and reduced wing aspect ratio to keep wing span constant); 5) wing moved backward to reduce cabin noise, and to keep rotating engine parts out of the cabin area; 6) horizontal tail plane in canard configuration (and with a fuel trim tank) as a result of wing position; 7) slight modifications in fuselage geometry to better accommodate the new wing and the canard, and minor changes in cabin layout to provide ground service access to galleys and toilets.

The analysis presented here consists of the application of PrADO to the LNA in the design analysis mode. Because of the configuration features mentioned in the preceding paragraph, handbook methods cannot be expected to produce useful results for several disciplines. Subsequently, the multiple lifting line method is selected to compute the aerodynamic characteristics. Mission range and fuel estimation are performed with flight simulation, considering the trimmed flight condition. Required static thrust estimation is done using a thermodynamic cycle simulation and a scalable "rubber" engine. For structural weight estimation, the finite element method described in Sec. II is used. The noise characteristics of this configuration are still under study at DLR. Therefore, no noise source description is available and the noise propagation module cannot be applied in this study.

For structural sizing with SAM, the two different discretizations of aircraft geometry needed are automatically generated by the MMG, as shown in Fig. 7. Note that the aerodynamic panel model also includes wake surfaces behind each part, which are not shown in the figure for clarity. The FE model features all relevant parts of the structure, including wing center box, keel beam, pressure bulkheads, cabin floor structures, and engine pylon structure.

Overall results for the LNA, compared with a conventional reference aircraft designed for the same transport mission (shown in Fig. 8), indicate that the LNA has both higher operational empty weight (OEW) and higher mission fuel weight (MFW), leading to a higher maximum takeoff weight (MTOW). In a conventional cost model, and with all operational parameters kept constant, higher weight and higher fuel consumption result in higher direct operating costs. These results are shown in Fig. 9. It can be assumed that the OEW increase is substantially caused by the increase both in fuselage

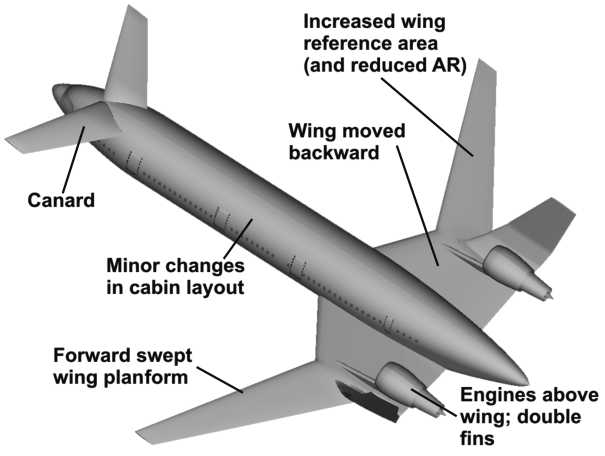

Fig. 6 LNA geometry model and configuration features.

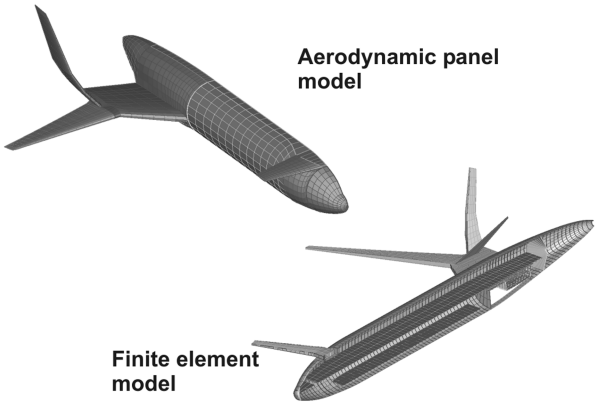

Fig. 7 MMG models for the LNA.

Fig. 8 Reference aircraft geometry model.

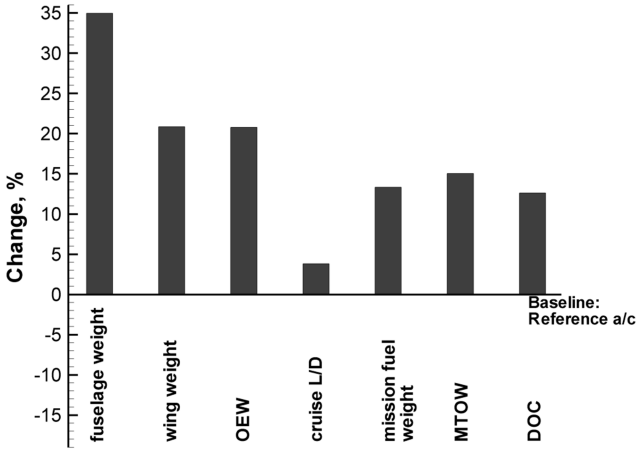

Fig. 9 Results of PrADO design analysis, LNA compared with reference aircraft.

and wing structural weight. An in-depth analysis of factors influencing structural sizing for the LNA configuration has been performed and is presented in [16]. The main findings of this analysis are summarized here. For the wing, the weight increase of roughly 20% is in good agreement with the increase in reference area (+28%). It is less than linear because the larger wing has a higher thickness at the root, thus alleviating stresses resulting from wing bending loads. For the fuselage, the weight increase of 35% is, at first sight, hard to explain, because fuselage geometry and cabin layout change only slightly between the LNA and the reference aircraft. A deeper insight can be gained, however, from the results of FE-based sizing. The load cases used for structural sizing include seven flight cases and two landing impact cases at maximum landing weight, one with maximum possible fuel and one with maximum possible payload. In SAM's nomenclature, the flight cases are referred to as load case numbers 1, 4, 5, 6, 7, 8, and 9, whereas the landing impact cases have the numbers 2 and 3. Figure 10 shows a plot of the critical load case for each element, both for the reference aircraft and the LNA. As can be seen, the fuselage of the reference aircraft converges mostly at minimum wall thickness (white), whereas some elements near the wing root are driven by load case number 4, a high-speed 2.5g maneuver load case. For the LNA, however, load case number 3 (landing impact with maximum payload) becomes the predominant load case for sizing of the fuselage structure. It can be shown that the LNA fuselage is highly affected by bending moments which result from the distance between the fuselage center of gravity (c.g.) and the load transfer point between the fuselage and the wing (where the resulting aerodynamic lift or landing gear forces are localized). These bending moments are most demanding during landing impact because of the high load factor (i.e., vertical acceleration) associated with it.

This is an important result. Empirical methods normally used in preliminary design (e.g., Burt–Phillips [9]) are not capable of reproducing this effect because they are calibrated with data for conventional aircraft configurations. The FE results show, however, that any measures aimed at reducing LNA weight will be increasingly successful the more they contribute to a reduction of fuselage bending loads. Three possible measures are discussed in [16]. One of these measures is a reduction of the cargo hold size. Because of the configuration changes, the cargo hold of the LNA is larger than that of the reference aircraft and thus larger than it needs to be. Reducing its size gives the opportunity to move it as far back in the fuselage as possible and thereby to reduce bending loads. The second measure consists of increasing the maximum landing gear shock absorber and tire stroke. This makes the landing gear "softer" and reduces the load factor experienced during landing impact, thus reducing the overall load level. The third measure involves omitting the fuel trim tank in the canard. This moves the c.g. backward and reduces the loads that have to be carried through the fuselage. Results obtained by applying each of the three measures are shown in Fig. 11, using the original LNA as a baseline. In the first case, the cargo hold size has been reduced by 29% and is now the same as that of the reference aircraft. In the second case, the maximum landing gear stroke has been increased from 0.4 to 0.6 m, which is deemed as a feasible value for an aircraft this size. In the third case, the trim tank in the canard has simply been omitted. As can be seen, the first two measures influence the overall results in much the same way, although increasing landing gear stroke has an overall stronger effect. Fuselage weight decreases substantially, causing a noticeable reduction in OEW. Although cruise L/D (the relation between lift and drag as a basic parameter for aerodynamic efficiency) is also reduced as the lighter aircraft flies at a different point on its aerodynamic polar, MFW decreases due to the reduced weight. Overall, this leads to a reduction of MTOW. The reduction of wing weight is to be seen mostly as an indirect result of overall weight reductions. The third measure, the omission of the trim tank, seems to have a different influence, however. Although changes in component weights and OEW are rather small, cruise L/D increases substantially, causing a strong reduction in MFW and thus causing MTOW to decrease. The reason for this can be deduced from Fig. 12, which shows plots of aircraft c.g. position (X_{CG}) over time for cruise of the LNA, both with and without trim tank. The plots include the position of the aerodynamic center of the wing X_{NW} and the position of the aerodynamic center of the aircraft X_N, which are the same for both configurations. On the one hand, the aircraft c.g. has to remain in front of X_N at all times if static stability is required. This constraint is satisfied for the LNA with trim tank, although payload distributions are possible that lead to a small (but probably acceptable) degree of instability. For the LNA without trim tank, the aircraft c.g. is behind X_N, yielding an unstable configuration during most of the cruise flight. On the other hand, however, cruise L/D is improved when decreasing the static stability margin. Whether the degree of instability of the LNA without trim tank is acceptable or not depends on the flight control system and its capability for providing artificial stability, and would finally be a regulations issue rather than only a question of technical feasibility.

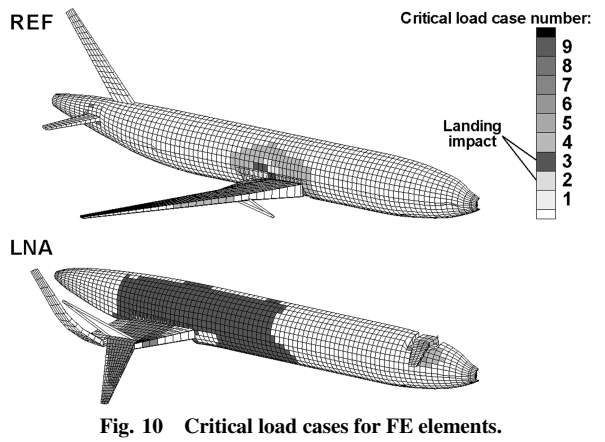

Fig. 10 Critical load cases for FE elements.

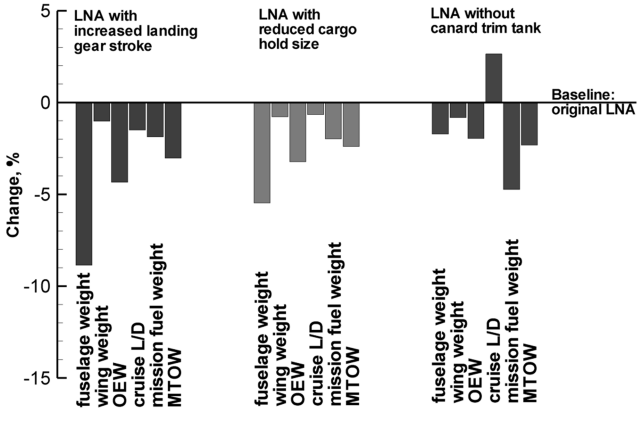

Fig. 11 Results of PrADO design analysis, LNA variants compared with original LNA.

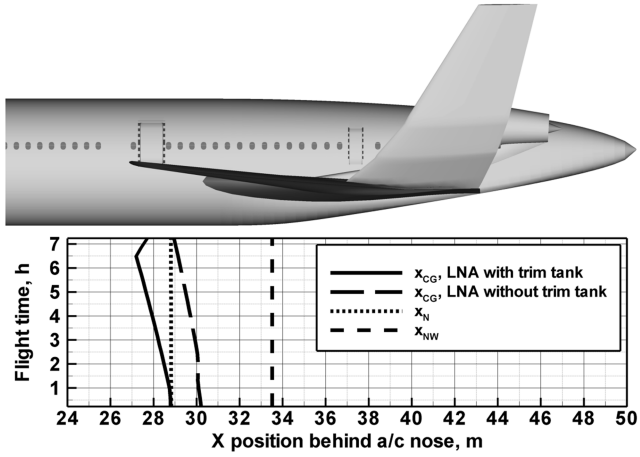

Fig. 12 LNA c.g. and aerodynamic center position during cruise flight.

2. Low-Noise Aircraft Stepwise Development

An advantage of the automated parametric design process is that it enables a different approach to the interpretation of results for the LNA, which focuses on the configuration features described previously, and is also studied in [11]. The idea is to start with the reference aircraft and to perform a step-by-step development into the LNA, adding one or two specific features at a time, leading to the following steps:

Step 0: The reference aircraft

Step 1: Step 0 + increased wing reference area

Step 2: Step 1 + LNA wing

Step 3: Step 2 + canard

Step 4: Step 3 + wing moved backward

Step 5: Step 4 + engines above wing+double fins instead of vertical tail plane

Step 6: Step 5 + LNA cabin layout and fuselage geometry

The corresponding geometry models are shown in Fig. 13. For all steps, the landing gear stroke is set at 0.6 m and the canard trim tank is omitted (where applicable), the effects of these measures being discussed previously. Apart from this, step 6 corresponds to the original LNA. For each of these steps, the PrADO input file is generated manually from the input file of the previous step by changing only the parameters pertaining to the indicated features. Then, a complete design analysis is performed for each step independently. Thus, the results for each step represent a converged design with minimum structural weight, minimum static thrust, etc. This approach makes it possible to visualize the influence that each configuration feature has on the overall results, although it should be kept in mind that the intermediate steps are not supposed to represent viable aircraft configurations. Furthermore, no optimization (e.g., of wing twist distribution) is performed for any step. Results are shown in Fig. 13, using step 0 as the comparison baseline. Again, a detailed discussion is given in [16] and is summarized here.

At step 1, the increase in wing reference area leads to an increase in wing weight as discussed before. Because the wing is now basically oversized for the aircraft, wing loading is reduced, leading to a decrease in cruise L/D and a subsequent increase in required MFW. At step 2, the main change from step 1 is an increase in cruise L/D, brought about by the new wing twist distribution and planform (which leads to a more favorable trimmed flight condition). As a result, MFW is slightly lower than for step 0. At step 3, the introduction of the canard leads to increased weight for the wing (due to canard downwash, which shifts the resulting lift force outward, increasing wing bending loads) and for the fuselage (due to bending loads caused by the aerodynamic load on the canard as well as the unfavorable integration of the canard in the pressurized cabin section). Cruise L/D decreases only slightly, but the increased OEW also causes an increase in required MFW, explaining the significant MTOW gain. Step 4 is dominated by the change in wing position, which causes an increase in fuselage bending loads and a massive increase in fuselage weight, as discussed. At the same time, the increasing distance between the wing and the canard reduces the effects of downwash on the wing (reducing its weight) and yields a more favorable trimmed flight condition, thus improving cruise L/D. At step 5, the main change with relation to step 4 is the increase in wing weight, caused by both the change in engine chordwise position and the introduction of the double fins. The former increases wing torsional moments, whereas the latter introduces new loads that have to be carried through the wing. Step 6, finally, shows only minor changes compared with step 5, confirming that the changes in fuselage geometry and cabin layout are of negligible influence.

This stepwise development, apart from illustrating the flexibility of the preliminary design process, shows that there is not one single reason for the LNA's high weight, but that each configuration feature of the LNA contributes to a certain extent to the total weight gain, the main influences being the increase in wing reference area, the introduction of the canard, and the rearward positioning of the wing. What becomes apparent is that, for the LNA, the high structural weight overrides any aerodynamic advantages that a canard configuration might inherently have.

3. Static Aeroelasticity

Another effect not usually considered in preliminary design is the influence of static aeroelasticity, the effects of which are shown in Figs. 14 and 15. In reality, an aircraft is not a rigid body, meaning that the different forces acting on the aircraft during flight cause an elastic deformation of its geometry. Aerodynamic forces, however, are influenced by the shape of the aircraft moving through the atmosphere. This creates an interdependency between the structure

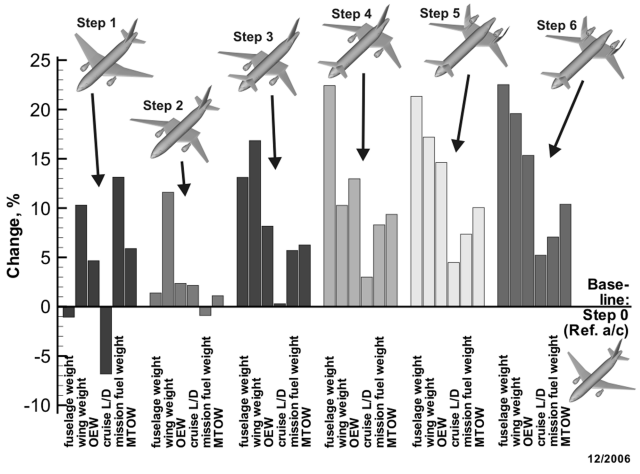

Fig. 13 Results of PrADO design analysis, LNA stepwise development.

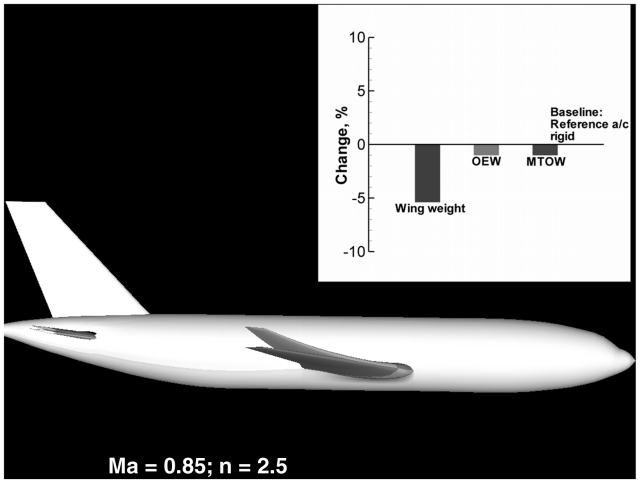

Fig. 14 Effects of static aeroelasticity, rearward swept wing.

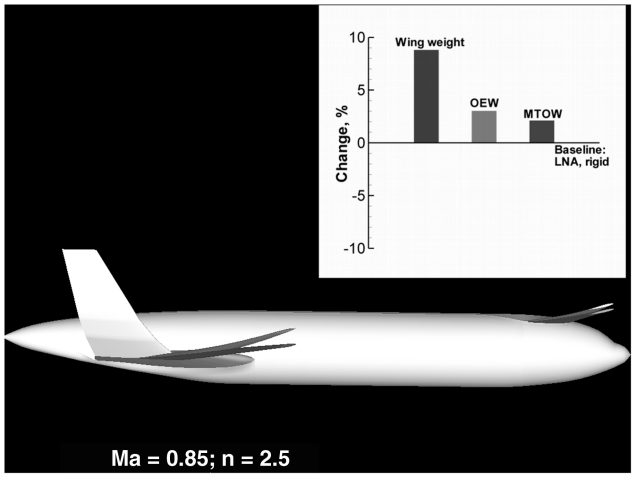

Fig. 15 Effects of static aeroelasticity, forward swept wing.

of an aircraft and its aerodynamic characteristics. For a conventional rearward swept wing, deformation in flight usually leads to a decrease of outer wing angle of attack, as shown in Fig. 14. As a result, aerodynamic load on the wing is shifted inward, reducing wing bending load and resulting in a lower wing weight compared with a rigid model (see box in Fig. 14). Neglecting this effect in preliminary design leads to an excessive weight prediction and is, in any case, a conservative assumption. For a forward swept wing, however, Fig. 15 shows that deformation in flight tends to increase outer wing angle of attack, thus shifting the aerodynamic load on the wing outward, increasing wing bending moment and causing an increase in wing weight (see box in Fig. 15). Neglecting this effect is no longer a conservative assumption, making it more important to consider static aeroelasticity for forward swept wings.

4. Configuration Optimization

Keeping in mind the effects of static aeroelasticity, the following analyses are nevertheless performed in rigid body mode. An optimized LNA concept can be derived by combining the three measures previously discussed. Because the omission of the canard trim tank has large effects on aircraft stability and because it is not clear whether the resulting degree of instability could be tolerated or not, two versions are to be analyzed. The configuration "LNA-opt-a" consists of the LNA with enhanced landing gear, reduced cargo hold size, and without trim tank; the configuration "LNA-opt-b" consists of the LNA with enhanced landing gear and reduced cargo hold size, but keeps the trim tank. For the comparison baseline, it has to be considered that one of the measures, namely, increasing maximum landing gear stroke, can also be applied to the reference aircraft. As can be seen in Fig. 16, in which results for the reference aircraft with a maximum landing gear stroke of 0.6 m are shown in comparison to results for the original reference aircraft (maximum stroke of 0.4 m),

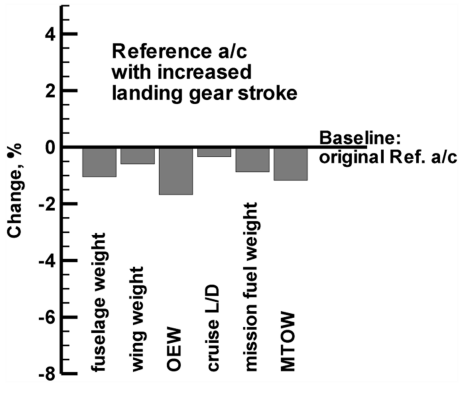

Fig. 16 Results of PrADO design analysis, reference aircraft with and without increased landing gear stroke.

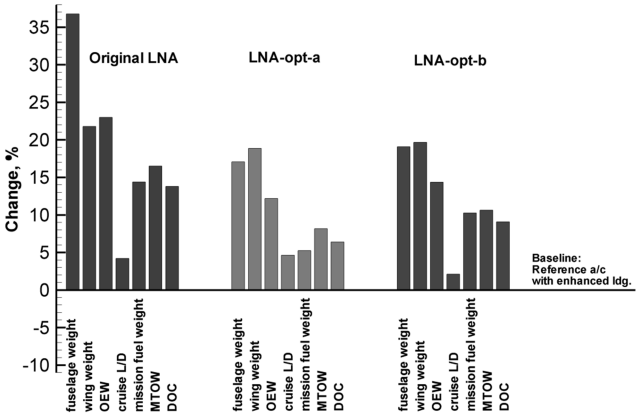

Fig. 17 Results of PrADO design analysis, optimized LNA versions vs optimized reference aircraft.

the overall changes in weight resulting from the landing gear enhancement are by far smaller than those obtained on the LNA (cf. Fig. 11). Nevertheless, this still represents an improvement of the reference aircraft, and the reference aircraft with enhanced landing gear is therefore used as comparison baseline in Fig. 17, where design analysis results for the original LNA and the two optimized LNA versions are presented. For both optimized versions, fuselage weight is significantly reduced in comparison to the baseline LNA, as a result of the measures intended to alleviate fuselage bending loads. Wing weight changes only slightly, however, as it is driven mainly by the increased wing reference area. OEW for both configurations is still more than 10% higher than for the reference aircraft, though. Although weight differences between both optimized LNA versions are only small, a major difference exists in cruise L/D (which is substantially higher for the LNA version without the trim tank) and subsequently in required MFW. For LNA-opt-a, MFW is moderately higher than for the reference aircraft despite the LNA's higher OEW. For the LNA version with the trim tank, cruise L/D is only slightly higher than that of the reference aircraft, leading to a stronger increase in MFW. In terms of DOC, both LNA versions have higher cost than the reference aircraft, as they are not only heavier but also consume more fuel, all other operational parameters being constant.

More insight into some of the design sensitivities can be gained from a closer look at the DOC results. Considering that the LNA configuration is intended to reduce the community noise impact, questions that arise include whether this goal can be achieved and what effect it could have on the operational economics of the aircraft. The first question must remain unanswered at this point, because the determination of noise characteristics for the LNA is beyond the scope of the analyses performed at IFL. However, if one is to assume that the LNA would indeed be significantly less noisy than the reference aircraft, potential effects in terms of DOC can already be made visible in the conventional DOC model implemented in PrADO. Two cases are conceivable for this:

1) The LNA is less penalized by nighttime flying restrictions due to its low noise.

2) The LNA can expect reduced landing charges at airports due to its low noise.

To explain how these two cases can contribute to cost reductions, it is necessary to discuss a few of the equations used in the DOC model. The basic equation of the model relates the total costs induced by the aircraft during its lifetime to the amount of revenue seat kilometers flown by the aircraft in its life cycle, as shown in Eq. (3).

$$\mathrm{DOC} = \frac{\sum C}{\sum \mathrm{RSKM}} = \frac{C_{\mathrm{A/C}} + C_{\mathrm{FUEL}} + C_{\mathrm{MRO}} + C_{\mathrm{CREW}} + C_{\mathrm{FEES}}}{N_{\mathrm{Pax}} \cdot R \cdot N_F} \tag{3}$$

The sum of costs C includes costs generated by the aircraft itself (purchase value, depreciation, insurance, spare parts procurement) $C_{\mathrm{A/C}}$, costs of fuel C_{FUEL}, costs of maintenance, repair, and overhaul

C_{MRO}, costs of cockpit and cabin crew C_{CREW}, and costs of fees and charges C_{FEES}. All of these costs are calculated so that they represent the total value for the whole life cycle of the aircraft. The total revenue seat kilometers (RSKM) are the product of the number of passengers on the aircraft N_{PAX}, a representative mission range R, and the amount of flights performed during the lifetime of the aircraft N_F.

$$N_F = \frac{u \cdot y^* \cdot V_C}{R} \tag{4}$$

N_F is calculated according to Eq. (4), where V_C is the cruise speed of the aircraft, y^* the number of years the aircraft remains in service, and u is the utilization of the aircraft (in hours per year). The utilization is a function of the maximum time available to operate the aircraft t_{max}, the turnaround time spent on the ground between flights (t_{GND}, and, again, range and cruise speed, as shown in Eq. (5).

$$u = \frac{t_{max}}{1 + (t_{GND} V_C / R)} \tag{5}$$

This is where the first case has its effect. The maximum possible value for t_{max} would be 8760 h/year, which is the total amount of hours available in 1 year (365 days of 24 h). The German airline Lufthansa uses a value of 4198 h/year [17], which accounts for flight time losses related to maintenance, repair, and overhaul (MRO), route planning, and nighttime flight restrictions. This value is also normally used for t_{max} in the PrADO DOC model. In a simple academic exercise, Fig. 18 shows the resulting DOC for LNA-opt-a (relative to the reference aircraft) as a function of t_{max}. For LNA-opt-a to have a DOC value equal to that of the reference aircraft, t_{max} would have to increase to approximately 4950 h/year, which would correspond to an increase in utilization of 18%. Whether this increase in utilization would be achievable in real-world operations is hard to judge, as it depends strongly on how the airline would operate the aircraft. It must also be kept in mind that not every airport currently has nighttime flying bans, and that airlines often avoid nighttime curfews at airports by departing in the evening and arriving in the morning. Nevertheless, noise restrictions at airports are expected to become more stringent in the future, with more airports introducing nighttime curfews. At the same time, the expected increase in air travel could, at some point, make nighttime operations necessary at many airports to provide enough airport capacity. In such an environment, aircraft noise would have definite economic implications, and a potential increase in aircraft utilization could strongly influence the DOC.

The second case postulates that the LNA would be rewarded for its low community noise impact through reduced landing charges at airports. In Eq. (3), landing charges are included in the costs of fees and charges C_{FEES}, which also includes dispatch charges, as shown in Eq. (6).

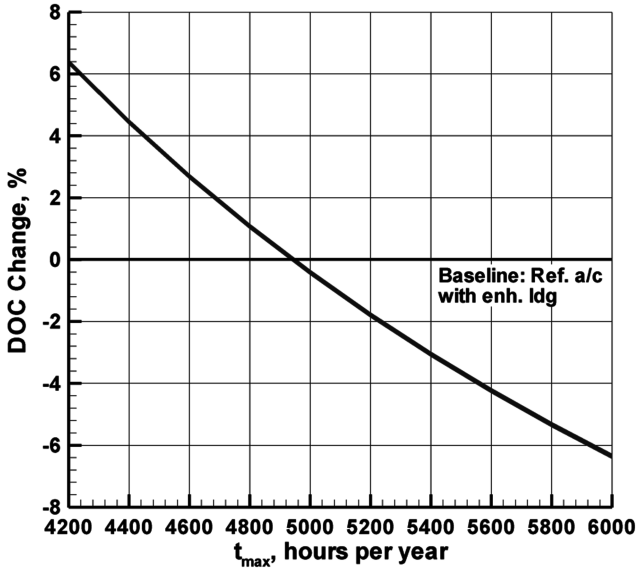

Fig. 18 DOC for LNA-opt-a with varying utilization.

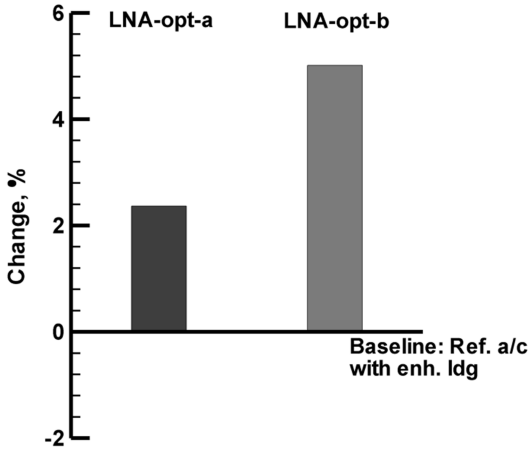

Fig. 19 DOC for optimized LNA configurations.

$$C_{FEES} = [c_{LDG} \cdot \text{MTOW} + c_{DISP} \cdot N_{PAX}] \cdot N_F \tag{6}$$

The total cost of fees and charges is influenced by specific cost factors for landing and dispatch (c_{LDG} and c_{DISP}, respectively). It becomes apparent that landing charges make up too small a portion of total DOC to enable DOC reductions in this case. Not only do they represent only a part of C_{FEES}, but C_{FEES} usually accounts for less than 10% of total DOC. Figure 19 shows DOC results for both optimized LNA versions with c_{LDG} set to zero (which eliminates landing charges), compared with the optimized reference aircraft with standard specific cost values. Even in this extreme, but unrealistic case, the total DOC for both LNA versions are still higher than those for the reference aircraft, indicating that they will always be higher regardless of the discount airports may offer to quiet aircraft on landing charges.

As can be seen from the two cases, whether an aircraft concept like the LNA is economically viable depends on the operational conditions it would encounter. In the given example, if the LNA were less penalized by nighttime flying restrictions, its chances of becoming economically viable would be greater than if the low community noise impact would be rewarded only by reduced landing charges. One conclusion that could be drawn from this is that the implementation of new technologies on future aircraft is likely not only to be a question of aircraft weight and performance, but also of regulation, certification, and the politic and economic environment that the aircraft may encounter; items that are very difficult to consider within a technically oriented design process. Both cases illustrate, however, that different parameters of an aircraft's operating environment can be considered in PrADO, and their effects on DOC can be made visible. With this, it becomes possible to assess the effects of changing the aircraft configuration, not only in terms of technical criteria (like weight), but also in terms of their economic consequences.

IV. Conclusions

The preliminary aircraft design and optimization tool is shown as a multidisciplinary, integrated, parametric, automated, and modular design tool which incorporates higher fidelity numerical methods for aerodynamic and structural analysis. Thanks to this, the tool is capable of producing a physically accurate representation of aircraft behavior and does not have to rely as heavily on empirical data as preliminary design processes usually do. This physically accurate representation, together with the multidisciplinary tool structure, forms the basis for successful application of the design process to unconventional aircraft configurations, as the presented application example clearly shows: effects like the significant increase in fuselage weight of this unconventional configuration would not be

predicted with empirical methods, but are clearly visible in the results of finite-element-based structural sizing.

The presented status of the design process is a solid basis for further development, which will focus on aspects of preliminary design that are especially relevant for environmentally friendly aircraft configurations. These include the completion of the noise propagation module with a parametric noise source model for airframe and engine noise, and the implementation of higher fidelity methods for the representation of conventional and unconventional high-lift devices.

Acknowledgments

The authors would like to thank L. Fornasier and European Aeronautic Defense and Space Company, military branch, Munich for providing the higher order subsonic/supersonic singularity method code. Thanks are also extended to M. Hepperle and C. Liersch at the Institute of Aerodynamics and Flow Technology of the German Aerospace Center, Brunswick, for providing the low-noise aircraft configuration.

References

[1] Sobieszczanski-Sobieski, J., and Haftka, R. T., "Multidisciplinary Aerospace Design Optimization: Survey of Recent Developments," *Structural and Multidisciplinary Optimization*, Vol. 14, No. 1, 1997, pp. 1–23. doi:10.1007/BF01197554

[2] Herrmann, U., Frhr. von Geyr, H., and Werner-Westphal, C., "Mixed Fidelity Multi Discipline Optimization of a Supersonic Transport Aircraft," AIAA Paper 2005-534, Jan. 2005.

[3] Heinze, W., "Ein Beitrag zur quantitativen Analyse der technischen und wirtschaftlichen Auslegungsgrenzen verschiedener Flugzeugkonzepte für den Transport großer Nutzlasten," Zentrum für Luft- und Raumfahrt Rept. 94-01, Technische Univ. Braunschweig, Brunswick, Germany, 1994.

[4] Heinze, W., Österheld, C. M., and Horst, P., "Multidisziplinäres Flugzeugentwurfsverfahren PrADO—Programmentwurf und Anwendung im Rahmen von Flugzeugkonzeptstudien," Deutsche Gesellschaft für Luft- und Raumfahrt, Paper DGLR-2001-194, Bonn, Germany, 2001.

[5] Österheld, C. M., Heinze, W., and Horst, P., "Influence of Aeroelastic Effects on Preliminary Aircraft Design," *Proceedings of the 22nd International Congress of Aeronautical Sciences*, International Council of the Aeronautical Sciences (ICAS), Harrogate, UK, 2000.

[6] Österheld, C. M., "Physikalisch begründete Analyseverfahren im integrierten multidisziplinären Flugzeugvorentwurf," Zentrum für Luft- und Raumfahrt Rept. 2003-06, Technische Univ. Braunschweig, Brunswick, Germany, 2003.

[7] Tecplot, Software Package, Ver. 10, Release 4, Tecplot, Bellevue, WA, 2004.

[8] Horstmann, K. H., "Ein Mehrfachtraglinienverfahren und seine Verwendung für Entwurf und Nachrechnung nichtplanarer Flügelanordnungen," Deutsche Forschungs- und Versuchsanstalt für Luft- und Raumfahrt Rept. DFVLR-FB 87-51, Brunswick, Germany, 1987.

[9] Burt, M. E., and Phillips, J., "Prediction of Fuselage and Hull Structure Weight," Royal Academy of Engineering Rept. 122, 1952.

[10] Fornasier, L., "HISSS: A Higher-Order Subsonic/Supersonic Singularity Method for Calculating Linearized Potential Flow," AIAA Paper 84-1646, 1984.

[11] Werner-Westphal, C., Heinze, W., and Horst, P., "Consideration of Aircraft Noise Propagation in Multidisciplinary Integrated Preliminary Aircraft Design," *Proceedings of the 8th Confederation of European Aerospace Societies: Aeroacoustics Specialists' Committee Workshop: Aeroacoustics of New Aircraft & Engine Configurations*, Budapest Univ. of Technology and Economics, Budapest, Nov. 2004.

[12] Westphal, R., "Untersuchungen zur Einbindung eines Lärmausbreitungsmodells in den integrierten Flogzeugvorentwurf," Student Project Rept. SA 715, Library of the Inst. of Aircraft Design and Lightweight Structures, Technische Univ. Braunschweig, Brunswick, Germany, 2004 (unpublished).

[13] Smith, M. J. T., *Aircraft Noise*, Cambridge Univ. Press, Cambridge, England, U.K., 1989.

[14] Gillian, R. E., "Aircraft Noise Prediction Program User's Manual," NASA TM 84486, 1982.

[15] "Noise Levels for U.S. Certificated and Foreign Aircraft," Federal Aviation Authority Advisory Circular AC 36-1H, 2001.

[16] Werner-Westphal, C., Heinze, W., and Horst, P., "Structural Sizing for an Unconventional, Environment-Friendly Aircraft Configuration Within Integrated Preliminary Design," Deutsche Gesellschaft für Luft- und Raumfahrt, Paper DGLR-2006-119, 2006.

[17] Pohl, H. W., "Ein Beitrag zur quantitativen Analyse des Einflusses von Auslegungsparametern auf den optimalen Entwurf von Verkehrsflugzeugen," Ph.D. Dissertation, Faculty of Mechanical and Electrical Engineering, Technische Univ. Braunschweig, Brunswick, Germany, 1987.